The Journal of Chemical Physics

In situ identification of surface sites in Cu–Pt bimetallic catalysts: Gas-induced metal segregation

Cite as: J. Chem. Phys. **157**, 234706 (2022); https://doi.org/10.1063/5.0130431
Submitted: 11 October 2022 • Accepted: 02 December 2022 • Published Online: 19 December 2022

Tongxin Han, Yuanyuan Li, Yueqiang Cao, et al.

The Journal of Chemical Physics ARTICLE scitation.org/journal/jcp

In situ identification of surface sites in Cu–Pt bimetallic catalysts: Gas-induced metal segregation

Cite as: J. Chem. Phys. 157, 234706 (2022); doi: 10.1063/5.0130431
Submitted: 11 October 2022 • Accepted: 2 December 2022 •
Published Online: 19 December 2022

Tongxin Han,[1] Yuanyuan Li,[2,a)] Yueqiang Cao,[3] Ilkeun Lee,[1] Xinggui Zhou,[3] Anatoly I. Frenkel,[2,4] and Francisco Zaera[1,b)]

AFFILIATIONS

[1] Department of Chemistry and UCR Center for Catalysis, University of California, Riverside, California 92521, USA
[2] Department of Materials Science and Chemical Engineering, Stony Brook University, Stony Brook, New York 11794, USA
[3] State Key Laboratory of Chemical Engineering, School of Chemical Engineering, East China University of Science and Technology, Shanghai 200237, China
[4] Chemistry Division, Brookhaven National Laboratory, Upton, New York 11973, USA

Note: This paper is part of the JCP Special Topic on *In Situ* and Operando Characterization.
[a)] **Present address:** Chemical Sciences Division, Oak Ridge National Laboratory, Oak Ridge, TN 37831, USA.
[b)] **Author to whom correspondence should be addressed:** zaera@ucr.edu

ABSTRACT

The effect of gases on the surface composition of Cu–Pt bimetallic catalysts has been tested by *in situ* infrared (IR) and x-ray absorption spectroscopies. Diffusion of Pt atoms within the Cu–Pt nanoparticles was observed both in vacuum and under gaseous atmospheres. Vacuum IR spectra of CO adsorbed on $CuPt_x$/SBA-15 catalysts ($x = 0–\infty$) at 125 K showed no bonding on Pt regardless of Pt content, but reversible Pt segregation to the surface was seen with the high-Pt-content ($x \geq 0.2$) samples upon heating to 225 K. *In situ* IR spectra in CO atmospheres also highlighted the reversible segregation of Pt to the surface and its diffusion back into the bulk when cycling the temperature from 295 to 495 K and back, most evidently for diluted single-atom alloy catalysts ($x \leq 0.01$). Similar behavior was possibly observed under H_2 using small amounts of CO as a probe molecule. *In situ* x-ray absorption near-edge structure data obtained for $CuPt_{0.2}$/SBA-15 under both CO and He pointed to the metallic nature of the Pt atoms irrespective of gas or temperature, but analysis of the extended x-ray absorption fine structure identified a change in coordination environment around the Pt atoms, from a (Pt–Cu):(Pt–Pt) coordination number ratio of ~6:6 at or below 445 K to 8:4 at 495 K. The main conclusion is that Cu–Pt bimetallic catalysts are dynamic, with the composition of their surfaces being dependent on temperature in gaseous environments.

I. INTRODUCTION

Much heterogeneous catalysis, including most hydrogenations of organic feedstocks, relies on the use of late transition metals.[1–3] Pt, Pd, and Rh in particular are quite active and are used extensively for a variety of industrial processes. Unfortunately, late transition metals are not very selective and tend to hydrogenate most if not all of the double and triple bonds in organic molecules with multiple unsaturation. To add flexibility to the design of selective metal-based catalysts, two or more metals can be mixed to create alloys. Bi- and multi-metallic catalysts have been used extensively for decades;[4–6] mixed metals may display unique electronic properties, often (but not always) a weighted average of the electronic properties of the individual components,[7–10] and/or mixed-metal ensembles of atoms on the surface with unique catalytic properties.[11–13]

A new version of alloying in catalysis has gained attention in recent years where a majority metal is mixed with a small amount of a second component to create so-called single-atom alloys (SAAs).[14–17] The difference with other more traditional bimetallic catalysts is that, in SAA, the minority component is believed to be present on the surface of the nanoparticles (NPs) in isolated form, far from other atoms of the same metal. The premise guiding the design of SAA catalysts is that the single-atom sites add specific

functionality lacking in the majority component, which otherwise is assumed to selectively promote the process of interest.[17,18] In the case of hydrogenation catalysis, for instance, the addition of small amounts of an active metal such as Pt or Pd may help with the activation of molecular hydrogen, something for which coinage metals such as Cu or Au are not effective;[19–21] this way, it may be possible to exploit the presumed selectivity of those coinage metals for the promotion of the hydrogenation steps.[16,17,22–25]

Empirically, it has become clear that SAA catalysts can, in many instances, improve the selectivity of hydrogenation reactions.[26–31] An understanding of how that occurs, however, is still being developed. Much elegant surface-science work using model metal surfaces such as single crystals and controlled ultra-high vacuum (UHV) environments has been performed[27,32–34] and complemented with quantum mechanics calculations[35–37] to support a proposed mechanism by which H_2 molecules are dissociated on individual Pt or Pd atoms present on the surface, after which the resulting adsorbed H atoms spill over to the Cu or Au surfaces where the organic molecules are hydrogenated. On the other hand, more recent evidence from our group[30] and from others[23,38,39] has suggested that the performance of SAA catalysts under realistic catalytic conditions may be affected by additional factors, in particular the ease with which specific metals segregate to the surface and/or diffuse into the metal bulk upon exposure to various chemical environments.[30,38,40–44]

The fact that one of the metals in alloys may segregate to the surface or diffuse into the bulk depending on the reaction conditions and the chemical environments is well known; a beautiful example was provided some years ago by the Salmeron group, who showed, using near-ambient-pressure x-ray photoelectron spectroscopy (NAP-XPS), that Rh–Pd core–shell NPs undergo reversible changes in composition and chemical state in response to oxidizing or reducing conditions: Rh segregates to the surface in a pure NO environment, whereas a more mixed-metal layer with significant amounts of Pd on the surface develops during NO + CO conversions.[45] In another case, involving the selective hydrogenation of cinnamaldehyde, a Rh–Au bimetallic catalyst was shown to undergo segregation and form Janus NPs during catalysis.[46] If the active metal in SAAs was to diffuse deep into the bulk, its activity may be hindered. For instance, the group of Crooks and co-workers proved that coating Pt NPs with a layer of Cu, to form Pt@Cu core–shell structures, leads to the inhibition of the electrochemical hydrogen evolution reaction (HER).[47] Also, in a recent study by Frenkel *et al.*, pretreatment of a catalyst consisting of Pd–Au nanoparticles with 8% Pd was shown to result in its restructuring via segregation and formation of Pd dimers and trimers within the Au surfaces in an O_2 atmosphere vs fragmentation of the ensembles into Pd monomers (SAAs) in a H_2 atmosphere, a change that affected its H-D exchange activity.[48] Because of this potential change of surface composition in bimetallic catalysts under reaction conditions, it is imperative to characterize its composition *in situ* to determine the true nature of the active sites. In this work, we do that for the case of Cu–Pt bimetallic catalysts by combining the use of *in situ* infrared absorption (IR) and *in situ* x-ray absorption (XAS) spectroscopies during exposures to atmospheric pressures of different gases, both reactive (CO, H_2) and inert (He). Our results indicate that, indeed, selective metal segregation does occur as a function of temperature. The details are provided below.

II. METHODS

A total of 10 Cu–Pt bimetallic catalysts, denoted $CuPt_x$/SBA-15, were prepared by incipient wetness impregnation using copper nitrate ($Cu(NO_3)_2 \cdot 3H_2O$, Sigma-Aldrich, 98% purity) and chloroplatinic acid ($H_2PtCl_4 \cdot 6H_2O$, Sigma-Aldrich, ≥37.50% Pt basis) as the metal sources, as reported previously.[30,31] In our nomenclature, x represent the molar fraction of Pt added to a constant 5 wt. % Cu load and was varied from 0 (pure Cu) to ∞ (pure Pt). For instance, the $CuPt_{0.2}$/SBA-15 catalyst contains 5 wt. % Cu plus an additional 0.2 molar fraction of Pt relative to that Cu, which, given the atomic masses of Cu (63.546 g/mol) and Pt (195.084 g/mol), corresponds to a 3.1 wt. % Pt load. All catalysts were reduced at 625 K under H_2 for 3 h prior to their use. The NP average size was determined to be ~6 nm in most SAA cases (details provided in the supplementary material), and high-resolution transmission electron microscopy (HRTEM) images attested to the random distribution of the Pt atoms within the Cu NPs. A more detailed description of the physical characterization and pretreatment of these catalysts has been provided before.[30,31]

The transmission Fourier-transform infrared (FTIR) spectra of carbon monoxide adsorbed on the $CuPt_x$/SBA-15 catalysts were obtained using a homemade quartz IR cell capable of sustaining pressure of up to ~2 bars and of cooling or heating to temperatures within the range from 125 to ~700 K, and a Bruker Tensor 27 FTIR spectrometer equipped with a deuterated triglycine sulfate (DTGS) detector.[49,50] About 15 mg of the catalyst was pressed into a self-supporting wafer, placed in the center of the transmission IR cell, and reduced *in situ* at 625 K under 500 Torr H_2 for 3 h. For the experiments carried out under vacuum, the cell was evacuated and cooled down to 125 K (using liquid nitrogen), after which the sample was exposed to 50 Torr of CO (Matheson Tri-Gas, ≥99.5% purity) for 0.5 h and the cell was then evacuated for 10 min. Spectra were recorded from 125 to 475 K at 20 K intervals as the sample and cell were warmed up, and corrected using background traces obtained under the same condition before adsorption. For the *in situ* CO IR titration experiments, the cell was cooled down to room temperature and evacuated, after which an initial IR spectrum was taken to be used as the background reference. The CO gas was introduced to the appropriate pressure, and the indicated sequences of exposures and data acquisition followed. Reference spectra for the gas-phase CO were acquired by following the exact same procedure but without any catalyst in the IR cell. All spectra were acquired with a resolution of 2 cm^{-1}, and correspond to averages of 16 scans.

The *in situ* x-ray absorption spectroscopy (XAS) experiments were carried out at the Inner-Shell Spectroscopy (ISS) beamline of the National Synchrotron Light Source II (NSLS-II) of Brookhaven National Laboratory. Approximately 25 mg of the catalyst was loaded onto a quartz tubing (O.D. = 2.4 mm, I.D. = 2 mm) and mounted in a Clausen cell.[51] Initial Cu and Pt *in situ* XAS spectra were acquired under a flowing atmosphere of pure He (20 ml/min) for reference, after which the gas feed was switched to pure H_2 to reduce the catalyst, and then to the gases indicated in the reported experiments, all at 1 atm: pure H_2 (20 ml/min), pure He (10 ml/min), or 25 vol. % CO in He (20 ml/min total) were used as indicated. In all cases, the Pt L_3-edge XAS data were collected in fluorescence mode and the Cu K-edge (taken but not reported here) XAS data were collected in transmission mode. The XAS data were analyzed using

the Athena software. For the Cu K edge data, only the Cu–Cu path was used (the incorporation of an additional Cu–Pt was attempted but proved to have a negligible contribution to the signal), whereas for the Pt L_3 edge both Pt–Pt and Pt–Cu paths were included. The following constrains were added: ΔE_0(Pt–Pt) = ΔE_0(Pt–Cu) and N(Pt–Pt) + N(Pt–Cu) ≤ 12 (applied only if the sum is larger than 12). More details are provided in the supplementary material.

III. RESULTS

An early indication that exposure of $CuPt_x$/SBA-15 catalysts to different gas environments may lead to metal segregation was provided by *ex situ* IR characterization experiments using carbon monoxide as a probe.[30] Figure 1 displays the IR spectra obtained in the C–O stretching region for all of our ten catalysts after saturation with CO at 125 K. The data were acquired under vacuum, after pumping the CO used for dosing, while the IR cell was slowly heated; the four panels provide results for four different temperatures (125, 225, 325, and 425 K). As shown in Fig. 1, at low temperatures the main peaks for CO adsorbed on all of the $CuPt_x$/SBA-15 SAA catalysts (x = 0.001–0.75) are at frequencies in the 2100–2135 cm^{-1} (main feature) and 2157–2170 cm^{-1} (shoulder) ranges, blueshifted as the Pt content in the catalysts is increased. These values are close to those seen with the pure Cu/SBA-15 catalyst (~2124 and ~2160 cm^{-1}; Fig. 1, left panel, top trace) and far from the much larger feature seen with the pure Pt/SBA-15 catalyst (2097 cm^{-1}; Fig. 1, left panel, bottom trace). In fact, no signal that can be ascribed to CO adsorption on Pt atoms is seen in any of the alloy catalysts, with the possible exception of the broad feature seen around 2070 cm^{-1} with the $CuPt_{0.75}$/SBA-15 sample. It is concluded that no Pt atoms are present on the surfaces of any of the $CuPt_x$/SBA-15 (x ≤ 0.5) within the detectability limit of the IR technique. In terms of the oxidation state of the Cu surface, we have, on the basis of the extensive studies available in the literature,[52–57] assigned the main 2124 cm^{-1} peak and the 2160 cm^{-1} shoulder to adsorption on metallic and oxidized Cu, respectively;[57] it would appear that the catalysts are not yet fully reduced at the start of these experiments (they do become fully reduced upon heating in the presence of CO, see below).

Heating to 225 K leads to some noticeable changes (Fig. 1, second-from-left panel). For one, the high-frequency peak associated with adsorption on oxidized Cu is no longer evident in the spectra. It could be argued that CO bonding to those sites is weak and that, therefore, molecular desorption takes place at low temperatures, below 225 K. Alternatively, adsorbed CO may react with the surface oxygen atoms and form CO_2, thus reducing the surface; the fact that the IR signal for gas-phase CO_2 increases upon heating of these samples (not shown) leads us to favor this second explanation. In any case, some CO desorption from metallic CO also occurs by 225 K, since the intensity of the main peak from all Cu/SBA-15 and $CuPt_x$/SBA-15 catalysts decreases. Particularly noteworthy is the evolution of a new peak in the low-frequency range for the samples with high (x ≥ 0.2) Pt loads: that feature is weak and detected at 2050 cm^{-1} in $CuPt_{0.2}$/SBA-15 but grows and redshifts with increasing Pt fraction in the bimetallic NPs, to 2045 cm^{-1} in $CuPt_{0.5}$/SBA-15 and to 2044 cm^{-1} in $CuPt_{0.75}$/SBA-15. This signal is most likely associated with CO bonded to Pt atoms, which must therefore segregate to the surface. Given that the observed frequencies are below the values reported for CO adsorption on either pure Pt surfaces (even at low coverages)[58–60] or supported Pt catalysts,[61] we conclude that the Pt atoms in our bimetallic catalysts may be atomically dispersed within the Cu matrix. Similar frequencies have recently been reported for $CuPt_{0.39}/Al_2O_3$[62] and $AgPt_x/Al_2O_3$[63] SAA catalysts.

The third panel in Fig. 1 shows the IR spectra recorded after heating to 325 K. By this temperature, most of the CO adsorbed on Cu is gone (notice the change of scale between the first two and the last two panels in Fig. 1); the binding energy of CO on pure Cu/SBA-15 is on the order of ΔH_{ads} = −82 kJ/mol, and desorption

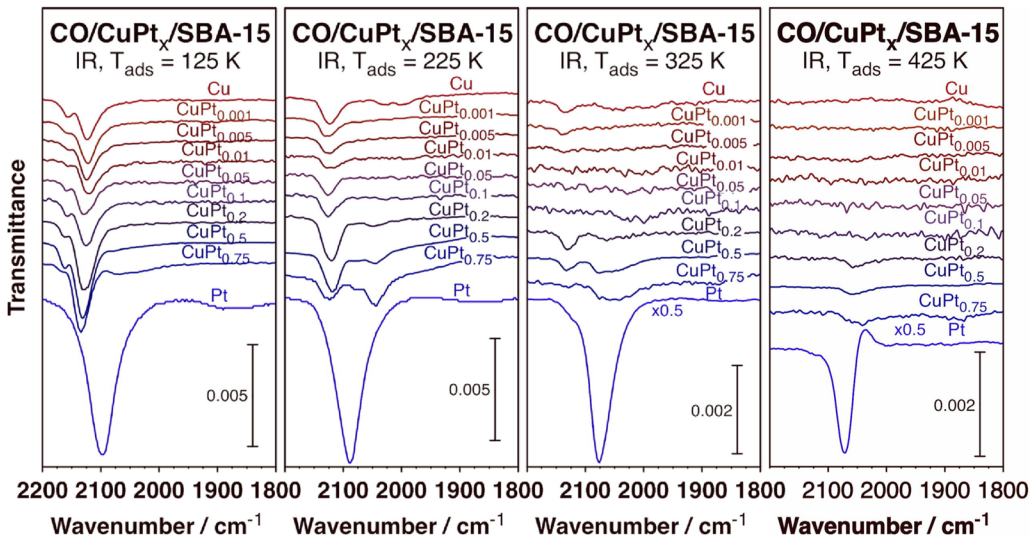

FIG. 1. IR spectra for CO adsorbed on 10 different $CuPt_x$/SBA-15 catalysts (x = 0–∞) as a function of temperature: data for four values of T (125, 225, 325, and 425 K) are provided, each in a separate panel.

in that case peaks at 245 K.[57] A small amount of CO on Cu is still detectable in some of the $CuPt_x$/SBA-15 samples, and the peak for CO adsorption on Pt sites in the high-content bimetallic catalysts broadens and blueshifts, possibly because the molecules no longer interact with other CO molecules bonded to adjacent Cu sites. Finally, by 425 K (Fig. 1, right panel), only small peaks for CO bonded to Pt are seen, and only for the high-Pt-content cases (at 2058 cm^{-1} with $CuPt_{0.1}$/SBA-15 and $CuPt_{0.2}$/SBA-15, and at 2042 cm^{-1} with $CuPt_{0.75}$/SBA-15). It should be noted that the CO seen in these high-Pt-content catalysts, although persistent to higher temperatures than the CO adsorbed on Cu, still desorbs at temperatures below those seen on pure Pt/SBA-15; the Pt–CO binding in these catalysts is clearly stronger than that of Cu–CO in pure Cu catalysts, but not as strong as in non-alloyed Pt surfaces.[64]

In the end, the data in Fig. 1 evidence the ability of CO to draw the Pt atoms in $CuPt_x$/SBA-15 catalysts from the bulk to the surface as those are heated. Additional experiments were performed to test the reversibility of this behavior. Figure 2 shows the IR data collected with the $CuPt_{0.5}$/SBA-15 (top) and $CuPt_{0.75}$/SBA-15 (bottom) catalysts as they were saturated with CO and heated under vacuum three times in a row. The left panels show the results in the form of 3D "heat" plots: the x axis represents the frequency range and the y axis temperature, and the peak intensities are color-coded from low (blue) to high (red, with yellow for intermediate values); on the right side of Fig. 2, representative IR traces are provided for low (125 K) and high (225 K) temperatures for the three cycles. The spectra for the first cycle mimic those seen in Fig. 1 and demonstrate that, upon heating to 225 K or above, some CO adsorbed on Cu desorbs (all of the CO on the oxide sites plus approximately half of those on metallic Cu) and new Pt–CO sites develop, the consequence of Pt segregation to the surface. The data from the second cycle look similar to those from the first: upon cooling down the catalysts and saturating them again with CO the peaks for CO bonded to Cu reappear and the signals for adsorption on Pt go away, but heating to 225 K again leads to the desorption of CO from Cu–CO sites and to the re-segregation of Pt to the surface. The results recorded during the third cycle are somewhat different, pointing to a possible irreversible change in the Cu–Pt bimetallic NPs, but the general trends are still the same, namely, the dominance of CO adsorption on Cu is restored at low temperatures but gives way to CO bonding to segregated Pt after heating of the samples. Also to notice here is the observation that the Pt–CO still desorbs by 300 K, a temperature clearly higher than that for Cu–CO but much lower than when CO desorbs from pure Pt surfaces (≥350 K).[65–67]

The data presented so far were acquired *ex situ*, that is, under vacuum after having pumped the CO atmosphere from the IR cell. More relevant to the main goal of this project is the behavior of the Cu–Pt bimetallic NPs *in situ* in the presence of a gas phase. To achieve that, IR spectra were recorded under similar conditions, at different temperatures and in the presence of a fixed pressure of CO,

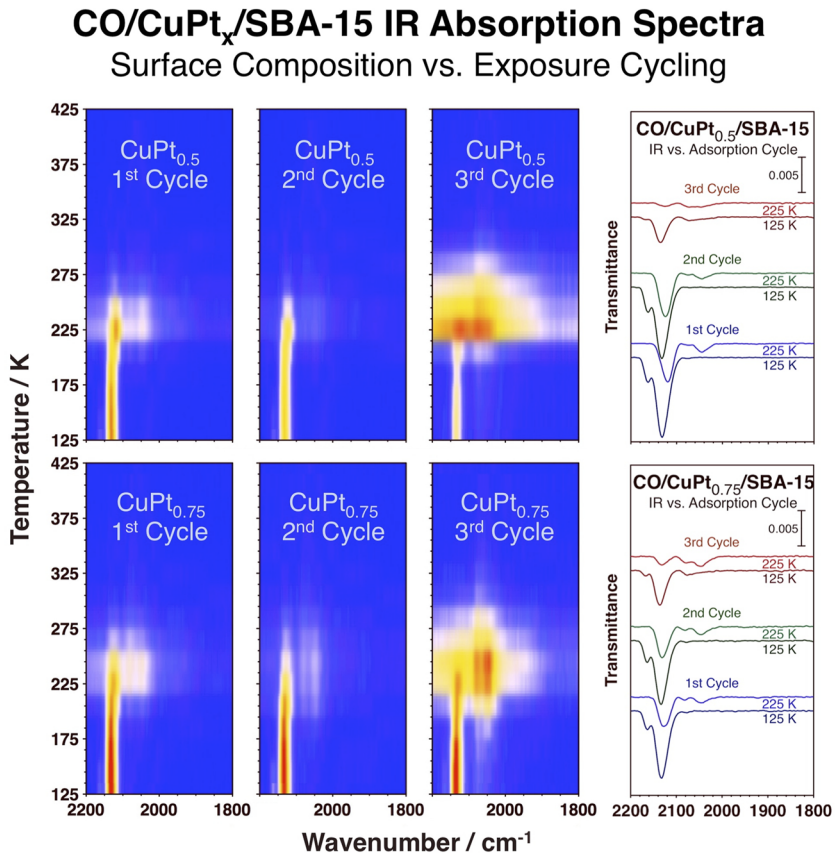

FIG. 2. IR spectra for CO adsorbed on $CuPt_{0.5}$/SBA-15 (top) and $CuPt_{0.75}$/SBA15 (bottom) catalysts recorded as a function of heating temperature during three dose-pump-heat cycles. The left panels correspond to 3D "heat" plots, whereas the right figures report representative spectra for low (125 K) and high (225 K) temperatures during each of the three cycles.

both in the presence and in the absence of the catalysts in the path of the IR beam. This way, the contribution from the gas-phase species detected in the latter could be subtracted directly from the former to extract the peaks attributable to the adsorbed species. This approach is feasible because when dealing with supported catalysts the area of the reactive surfaces is high and the total number of adsorbed molecules probed can reach values close to those of the gas-phase species. Figure 3 displays an example of the results acquired this way, in this case for the *in situ* titration of Cu and Pt sites in a $CuPt_{0.2}$/SBA-15 catalyst as a function of temperature using 10 Torr CO. Several features associated with the adsorbed species are seen (most clearly in the difference spectra provided in the right panel), in particular a peak at 2137 cm^{-1} at low temperatures (295 K) corresponding to adsorption on Cu surfaces. Interestingly, that feature slowly disappears with increasing temperature, presumably because CO binds weakly to Cu and desorbs at low temperatures, and is replaced by a new signal around 2050 cm^{-1} easily associated with Pt sites. A smaller and broader feature is already seen in this frequency region at low temperature, but the peak grows and sharpens at 495 K. It appears that the Pt atoms in the $CuPt_{0.2}$/SBA-15 catalyst, which may initially be located in the subsurface region, segregate to the surface at higher temperatures driven by the CO atmosphere. The broad peaks in the 2300–2400 cm^{-1} range correspond to gas-phase CO_2, some of which is made via a reaction of CO with surface oxygen in the partially oxidized Cu surface.

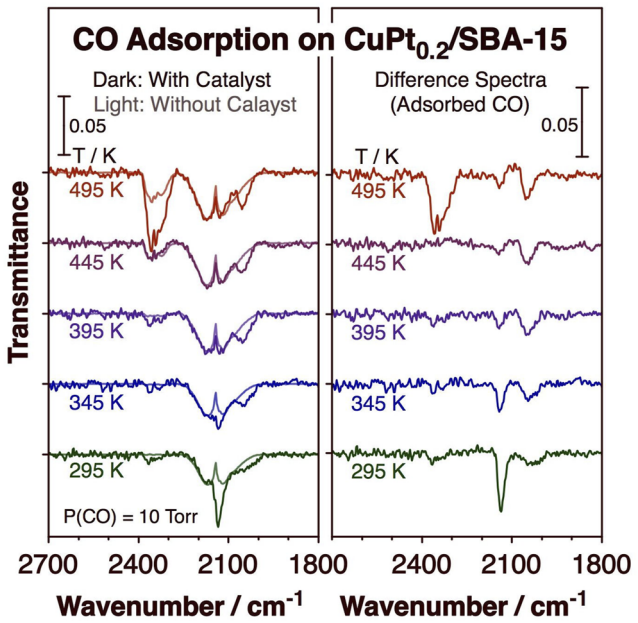

FIG. 3. Left: *In situ* IR spectra of CO adsorbed on a $CuPt_{0.2}$/SBA-15 catalyst as a function of temperature. The spectra were taken in the presence of 10 Torr of CO in the gas phase in order to maintain a steady-state coverage of adsorbed CO at the temperatures typical of catalytic processes. Additional reference spectra were acquired without the catalyst (light traces) in order to subtract the contribution from the gas phase to the spectra. Right: Difference spectra, to highlight the signals from the adsorbed species.

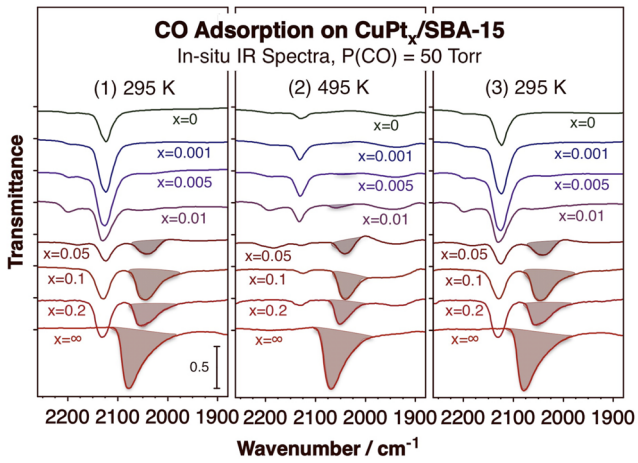

FIG. 4. *In situ* IR spectra of CO adsorbed on a family of $CuPt_x$/SBA-15 catalyst as a function of Pt content (x), in the presence of 50 Torr of CO in the gas phase (after subtraction of the gas-phase contribution). Three panels are provided, showing the traces recorded at 295 K (left), after heating to 495 K (center), and upon cooling back down to 295 K again (right). This temperature cycling was designed to test the reversibility of the changes seen as a function of temperature. Highlighted are the peaks corresponding to CO adsorbed on Pt sites.

Similar experiments were carried out with other $CuPt_x$/SBA-15 catalysts in order to characterize the behavior of our family of catalysts as a function of Pt content. Key results are displayed in Fig. 4: spectra recorded under 50 Torr CO at room temperature (left panel), after heating to 495 K (center), and after cooling back down to room temperature again (to test the reversibility of the temperature-induced changes; right) with eight catalysts, namely, the pure Cu/SBA-15 and Pt/SBA-15 cases and the $CuPt_x$/SBA-15 samples with x = 0.001, 0.005, 0.01, 0.05, 0.1, and 0.2. The spectra after subtraction of the gas-phase contribution are shown for clarity. Similar features to those reported in Fig. 3 were seen, namely, the peaks in the 2120–2130 and 2040–2080 cm^{-1} associated with CO bonding to Cu and Pt atop sites, respectively, and also an additional small feature at 2200 cm^{-1} most likely due to CO adsorption on oxidized Cu sites. A few trends become clear upon observation of this figure. For one, most (although not all) of the CO bonded to Cu desorbs by 495 K, due to the weak binding energy of those surface species. Not all of the CO is gone, however: the peak for Cu–CO retains ~20%–30% of its initial intensity in going from 295 to 495 K, a reflection of the equilibrium that is established between the adsorbed and gas-phase molecules. In fact, the steady-state CO surface coverage can be increased by increasing the gas-phase CO pressure, as we have already demonstrated for the case of Cu/SBA-15 in a previous publication[57] and as it can be seen in Fig. 5, to be discussed later.

The behavior of the IR peak associated with the Pt–CO species is somewhat different. With the more diluted alloys, for $x \leq 0.01$, the Pt content is low, and therefore the peak due to adsorption on Pt atoms is weak, as expected. What is significant is the fact that it is mostly seen at high temperatures, in the traces recorded at 495 K; the peaks at 2060 cm^{-1} (with $CuPt_{0.01}$/SBA-15) and 2035 cm^{-1} ($CuPt_{0.005}$/SBA-15) are most obvious in the spectra acquired while

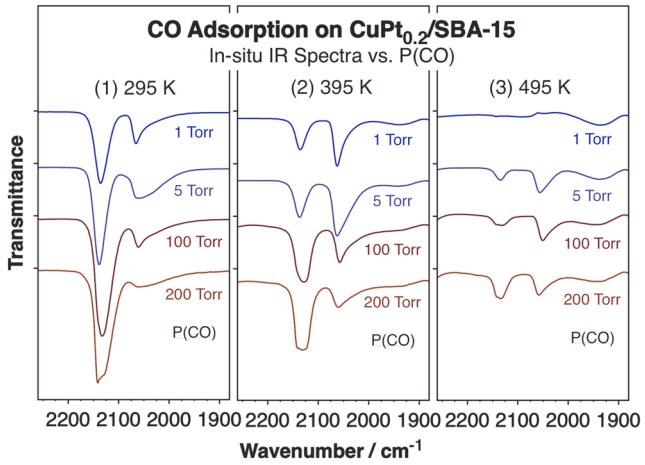

FIG. 5. *In situ* IR spectra of CO adsorbed on the $CuPt_{0.2}$/SBA-15 catalyst as a function of CO pressure (after subtraction of the gas-phase contribution). Three panels are provided, showing the traces recorded at 295 K (left), 395 K (center), and 495 K (right).

heating the reactor and go away again once the sample is cooled back down to room temperature. In addition, the value of those frequencies are low but do not follow the same trends seen with higher Pt content; notice in particular that the C–O stretching of the Pt–CO species in $CuPt_{0.01}$/SBA-15 (2060 cm^{-1}) is higher than with $CuPt_{0.05}$/SBA-15 (2035 cm^{-1}), in spite of the fact that the intensity of the peak in the former case is much lower than in the latter. The Pt surface atoms in the diluted bimetallic catalysts appear to behave differently than in the catalysts with higher Pt content and are likely to be isolated, as expected in SAAs. A previous study with $CuPt_x/Al_2O_3$ SAA catalysts identified the CO peak for adsorption on Pt redshifting from 2063 cm^{-1} for x = 1 to 2018 cm^{-1} for x = 0.033, after which no further shifting upon dilution was detected.[68] The most relevant observation here is the fact that, as already suggested by the *ex situ* IR experiments, adsorbed CO appears to help draw the Pt atoms toward the surface at high temperatures, and reversibly drive them back into the bulk at low temperatures.

For the alloys with high Pt content, $x \geq 0.05$, the peak position associated with CO bonded to Pt blueshifts significantly with increasing Pt content in the Cu–Pt bimetallic NPs, from 2040 cm^{-1} in $CuPt_{0.05}$/SBA-15 to 2070 cm^{-1} in Pt/SBA-15. These shifts are accompanied by related increases in peak intensity, due to increases in the surface coverage of Pt atoms, and can be explained by an increase in dipole–dipole intermolecular interactions, as has been reported and amply discussed in studies with Pt single crystals.[69–71] It seems that at these high Pt loadings CO behaves as in regular alloys with multi-atom Pt assemblies on the surface; these are not SAA catalysts. It is interesting to point out that the peak shifts seen in the IR feature for Cu–CO sites are less marked, suggesting that the surface chemistry of these catalysts is still dominated by the surface Cu atoms. It is also worth noticing that in Fig. 4 both the peak positions and the peak intensities of the feature for Pt–CO in the catalysts with $x \geq 0.05$ do not change significantly upon heating or cooling of the catalysts. Some sharpening and growth of that peak was seen in some cases, more clearly in the data in Fig. 3 (the data in Figs. 3 and 4 are from different experiments, performed at different CO pressures), but the changes are not as significant as with the more diluted alloys.

That lack of sensitivity of the IR features to changes in temperature with the high-Pt content catalysts was explored in more detail next. It was found that thermal treatment of the high-Pt-content catalysts in the presence of a gaseous atmosphere still leads to intermetallic atom mobility within the individual NPs, only that the behavior is complex as it depends on both temperature and CO pressure. This can be seen more clearly in Fig. 5, where CO IR spectra are shown for $CuPt_{0.2}$/SBA-15 as a function of temperature for several CO pressures. Peaks for both Cu–CO and Pt–CO sites are seen in all cases, but their absolute and relative intensities as well as their shapes change with varying conditions. The signals from the Cu–CO species go up in intensity with CO pressure and down with increasing temperature, both expected behavior. In the case of the Pt sites, however, the trends are reversed. Interestingly, in general, the peak for Pt–CO is more intense and sharper at the lower CO pressures, with the one exception of the 1 Torr CO at 495 K (in that case, the CO may have been consumed in oxidation reactions). These results suggest that at low temperatures higher gas pressures induce partial diffusion of Pt into the bulk of the bimetallic NPs. It is also seen that more surface Pt is detected in going from 295 to 395 K, following the same trend discussed above for the more diluted alloys, but then less Pt–CO is seen at 495 K. It could be thought that Pt may diffuse back into the bulk in this latter case, but in fact we believe that the observed behavior is the result of an equilibrium CO surface coverage change as the rate of CO desorption increases with T. In the end, the *in situ* IR data are all consistent with Pt diffusing into the bulk in the presence of CO at low temperatures and segregating back to the surface as the catalysts are heated.

The IR characterization of our Cu–Pt bimetallic catalysts has been carried out by using CO as a probe molecule, in a CO environment. CO is an important reactant in many catalytic processes, but is to be avoided in hydrogenation reactions. More relevant in those cases is the behavior of the surface of the catalyst under reducing conditions, H_2 atmospheres if possible. Unfortunately, adsorbed hydrogen is virtually invisible in IR, at least in supported catalysts [vibrational spectra taken using high-resolution electron loss spectroscopy (HREELS)[72,73] or inelastic neutron scattering (INS)[74–76] have been reported with some Pt systems]. Instead, an attempt was made here to test the performance of the $CuPt_x$/SBA-15 catalysts under hydrogen atmospheres in an indirect way. Two types of experiments were carried out (Fig. 6). In the first, the catalyst ($CuPt_{0.1}$/SBA-15 in this case) was first reduced in a H_2 atmosphere (200 Torr at 495 K) and then probed by adding a small amount of CO at room temperature (300 K; Fig. 6, left panel): after an initial addition of 0.2 Torr CO no adsorption could be detected, but upon adding another 0.2 Torr CO two peaks were clearly seen at 2127 and 2029 cm^{-1} corresponding to the C–O stretching mode of CO adsorbed on atop sites of metallic Cu and Pt surfaces, respectively. The interesting observation here is that the intensities of both features increase after each of two consecutive cycles of heating the sample from 300 to 495 K and cooling it back to 300 K. The growth of the peak for Cu explained by the CO reduction of the Cu_2O surface layer (that presumably was not fully removed during the H_2 treatment) and to the resulting creation of additional metallic Cu sites available for CO uptake; further confirmation of this interpretation is given by the growth of the peaks in the 2300–2400 cm^{-1} range

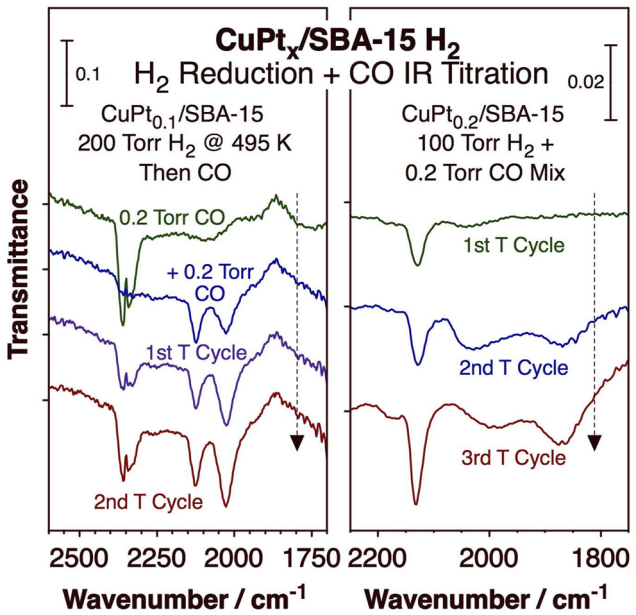

FIG. 6. IR spectra of CO adsorbed on $CuPt_x$/SBA-15 catalysts after different H_2 reduction treatments. Left: Spectra for $CuPt_{0.1}$/SBA-15 reduced in a 200 Torr H_2 atmosphere, after adding a small amount of CO (0.2 Torr twice) and cycling the temperature to 495 K and back to 300 K. Right: Data for $CuPt_{0.2}$/SBA-15 exposed to a 100 Torr H_2 + 0.2 Torr CO mixture; the spectra were obtained after each of three consecutive cycles of heating to 495 K and cooling back down to 300 K.

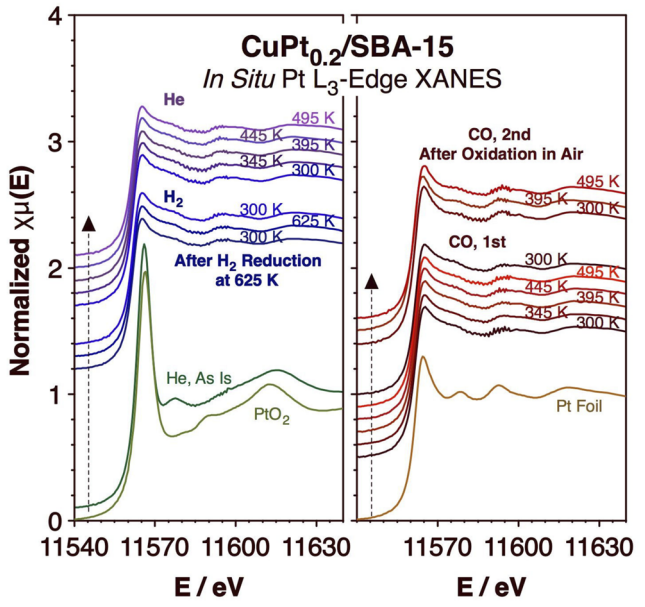

FIG. 7. *In situ* x-ray absorption near edge spectra (XANES) recorded around the Pt L_3 edge for a $CuPt_{0.2}$/SBA-15 catalyst exposed to different gases (H_2, He, CO) and cycled between 300 and 495 K. Reference spectra from PtO_2 (left) and a Pt foil (right) are also provided at the bottom for reference. No detectable changes in Pt electronic properties were seen in any case after initial reduction of the catalyst.

due to gas-phase CO_2, the product of CO oxidation. Importantly, the signal for the Pt–CO site, which grows faster relative to that for Cu–CO, suggests that H_2 may help draw the Pt atoms to the surface as a result of the high-temperature cycling.

The second set of experiments were done using gas mixtures of H_2 with traces of CO, 100 Torr H_2 + 0.2 Torr CO in the example shown in the right panel of Fig. 6 (which corresponds to the $CuPt_{0.2}$/SBA-15 catalyst). The peak at 2132 cm^{-1} for CO adsorption on metallic Cu is again seen to grow upon cycling to 495 K and back, a procedure that was carried out three times in this example. The same explanation applies to this system, namely, that the small amount of CO added to the H_2 gas helps complete the reduction of the metal NPs, removing the residual Cu_2O layer present on the surface under H_2 atmospheres at low temperatures. Unfortunately, in this case, adsorption on Pt atoms was not evident at any stage of the experiments (possibly because the CO was consumed by the surface reduction process). In the end, small amounts of CO were used in both examples in order to minimize its interference in the behavior of the catalyst under H_2 atmospheres, but a CO reducing effect was nevertheless identified. Some interference is unavoidable, more obviously perhaps in the second example, where the chances of surface site poisoning are greater. An alternative experimental approach is needed to better probe the surfaces of these catalysts *in situ* in atmospheres not containing CO.

We addressed this challenge by using XAS. XAS characterization of our catalysts can provide information on several aspects of their physical properties. In Fig. 7, we report data recorded *in situ* under different gas atmospheres in the x-ray absorption near-edge structure (XANES) region around the Pt L_3-edge in order to probe the electronic properties of the Pt atoms. The two low traces in the left panel of that figure contrast the spectra obtained for a $CuPt_{0.2}$/SBA-15 catalyst as is, before any pretreatment, vs that for a reference PtO_2 sample. The similarity between the two indicates that, initially, the platinum in our alloy catalyst is in an oxidized state, most likely Pt^{4+}. The match of the two spectra is not complete because of the dispersed nature of the Pt atoms within the Cu-based matrix in the supported NPs of the catalyst.

The reminder of the traces reported in Fig. 7 corresponds to the Pt L_3-edge XANES of the same $CuPt_{0.2}$/SBA-15 catalyst obtained after high-temperature (625 K) pretreatment in H_2, He, and CO. The data are grouped to highlight the behavior of the catalyst as they were subjected to heating–cooling cycles (from 300 K to 495 K and back) under different gas atmospheres: H_2 (left panel, third to fifth traces, counting from the bottom; heating in this case was cycled between 300 and 625 K), He (left panel, five top traces), and CO (right panel, second to sixth traces from the bottom). Interestingly, all these spectra look approximately the same, indicating that the electronic properties of the Pt atoms in the bimetallic catalyst are not significantly affected by the nature of the gas or the temperature (within the range tested here). Comparison with a reference spectrum obtained for a Pt foil (right panel, bottom) points to the fact that the Pt atoms are most likely in a zero-valent state; the peaks are seen at approximately the same energies, and their lower intensities can again be explained by the dilute nature of the Pt within the Cu-based alloy. Even after exposure to air (at room temperature, 30 min; right panel, top three traces), not much change is detected: a minor

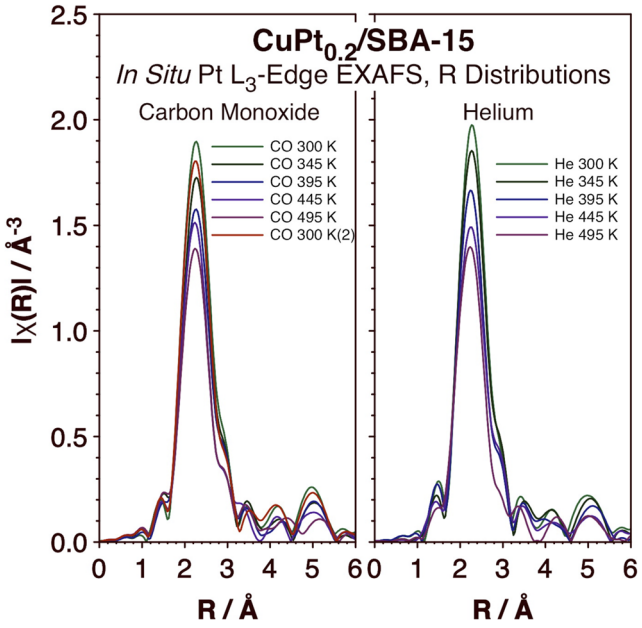

FIG. 8. Pt L_3-edge EXAFS radial distribution functions obtained for our $CuPt_{0.2}$/SBA-15 catalyst *in situ* in CO (left) and He (right) atmospheres as a function of temperature, which was cycled between 300 and 495 K.

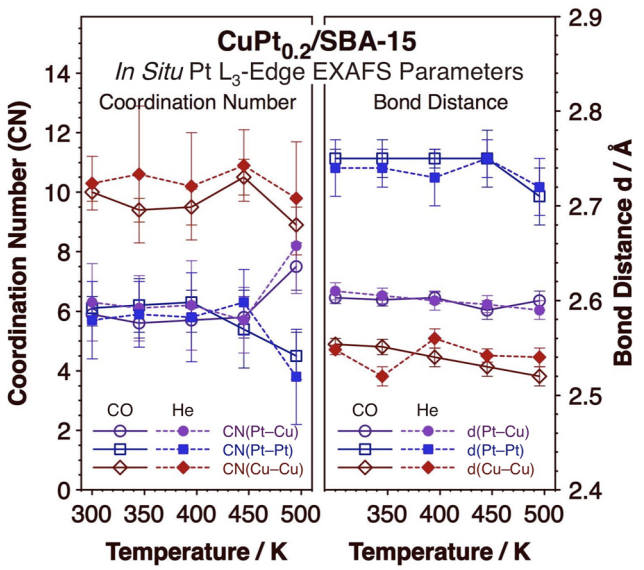

FIG. 9. Coordination numbers (CN, left panel) and bond distances (d, right panel) extracted from analysis of the EXAFS data obtained at the Pt L_3 and Cu K edges for the $CuPt_{0.2}$/SBA-15 catalyst under either CO or He environments, all as a function of temperature.

oxidation may be seen there, but the Pt atoms in that case are readily re-reduced to metallic Pt upon re-exposure to CO.

Additional information on the local environment surrounding the Pt atoms in our catalysts can be extracted from analysis of the extended x-ray absorption fine structure (EXAFS) region of the spectra in the Pt L_3-edge region. In Fig. 8, the EXAFS radial distributions functions (the Fourier transformation magnitudes of the k^2-weighted EXAFS spectra) are reported for the $CuPt_{0.2}$/SBA-15 catalyst while cycling the temperature from 300 to 495 K and back under CO (left panel) and He (right) atmospheres. In all cases, the main peak (uncorrected for the photoelectron phase shift) is seen at R ~ 2.23 Å, which corresponds to individual Pt atoms bonding to Cu neighbors; it suggests that the Pt is (partially) alloyed with Cu. A shoulder is also seen around 2.9 Å, pointing to the fact that some Pt atoms are directly bonded to other Pt atoms. The peak intensities decrease with increasing temperature, but that can be mostly accounted for by the so-called Debye–Waller factor that reflects the attenuation of x-ray scattering caused by thermal motion. Noticeably, similar behavior is seen in CO vs He atmospheres.

Figure 9 shows the results from processing of the EXAFS data to extract quantitative parameters on the coordination sphere around the Pt and Cu atoms, specifically on coordination numbers (left, CN) and bond distances (right, d) as a function of temperature under both CO and He atmospheres. Data were extracted from spectra for both the Pt L_3 and Cu K edges (the raw data for the Cu K edge are not shown). The coordination number around the Cu atoms hovers around 10–11 in all cases, almost all to other Cu atoms (red lines and symbols); attempts to add an additional Cu–Pt term to the fit of the radial distributions from the Cu K edge EXAFS data indicated that such contribution is negligible. The total coordination around the Cu atoms is lower than the value of 12 expected in bulk Cu, a reflection of the small size of the NPs leading to the existence of a detectable fraction of Cu atoms in lower-coordination surface sites. Using a back-of-the-envelope calculation starting with 6 nm spherical NPs (the average size of the NPs in our $CuPt_{0.2}$/SBA-15 sample),[31] where the fraction of atoms on the surface is estimated to be ~25%, and an average CN of 6 for those [it is 9 in the (111) plane] results in an average total CN of 10.5, within the range measured here. There is a slight decrease in CN at 495 K, which we associate with the higher coordination of Cu atoms to Pt atoms highlighted by the changes in CNs for Pt discussed next. The Cu–Cu bond distances are also within the value measured for bulk Cu (2.542 Å).

More relevant to our discussion is the environment surrounding the Pt atoms. Again, the behavior seen for those atoms as a function of temperature are similar in the CO and He atmospheres. In both cases, the coordination around individual Pt atoms is split about evenly, ~6:6, between Cu and Pt neighbors at temperatures up to 445 K. At 495 K, however, the Pt atoms are surrounded by a significantly larger number of Cu neighbors, at the expense of Pt–Pt pairs [(Pt–Cu):(Pt–Pt) ~ 8:4]. At the very least, this indicates some mobility of the Pt atoms within the bimetallic NPs induced by heating in the gaseous atmospheres. The changes also point to better Cu–Pt mixing at high temperatures, consistent with the CO IR data, and to partial segregation of Pt to the surface. The total CN around the Pt atoms adds up to ~12 in all cases, as expected for atoms in the bulk, but the lower values expected from having a fraction of the Pt atoms on the surface are within the experimental errors of the EXAFS data. There are still some Pt–Pt bonds in all cases, with bond distances slightly lower than that seen in the reference Pt foil (2.764 Å), and there also seem to be a slight contraction of that bond at 495 K. Incidentally, all of these changes proved to be reversible, as

the structural parameters return to the initial values upon cooling of the catalyst back to room temperature.

IV. DISCUSSION

The main purpose of this research has been to characterize the behavior of $CuPt_x$/SBA-15 bimetallic catalysts *in situ* in the presence of atmospheric pressures of reactive and non-reactive gases. Because of their potential use in selective catalysis, in particular to promote selective hydrogenation conversions, the chemistry of the Cu–Pt bimetallic surfaces has been characterized extensively under controlled vacuum conditions (as mentioned in the Introduction). However, much less is known about their performance under realistic catalytic conditions. It is well known that both temperature and the chemical environment can induce segregation of one or more components of metal alloys toward the surface, and if so, change the nature of the catalytic surface. In the case of single-atom alloy (SAA) catalysts in particular, the placement of the minority component, on the surface vs dissolved inside the bulk, is expected to determine the mechanism by which reactions occur on such catalysts. Here we have investigated the specific case of Cu–Pt bimetallics, but these issues are general. *In situ* characterization of SAA catalysts is required to develop a picture of the nature of the surface that promote the catalytic reactions.

One of the clear conclusions of this work is that, indeed, the presence of a gaseous atmosphere leads to the thermally promoted diffusion of Pt within the Cu–Pt bimetallic NPs. Even under vacuum a reactive gas such as CO can cause the segregation and/or desegregation of Pt atoms in those catalysts. Specifically, Fig. 1 shows that, at least for high-Pt-content $CuPt_x$/SBA-15 catalysts ($x \geq 0.2$), binding of CO to Pt atoms cannot be detected at 125 K but appears at temperatures as low as 225 K. This change indicates that the Pt atoms diffuse to the surface in between those two temperatures, likely aided by the presence of CO molecules on the surface. The binding of CO on the new sites is weaker than on pure Pt, but it is clearly stronger than on Cu/SBA-15. Another important observation regarding the changes of the $CuPt_x$/SBA-15 catalyst upon thermal cycling after exposure to CO is that the Pt segregation seen in Fig. 1 is reversible; cooling the catalysts back down to room temperature followed by CO re-dosing leads to the disappearance of the IR features associated with CO adsorption on Pt (Fig. 2). By and large, this behavior is reproduced in multiple CO-dosing/heating cycles.

A similar behavior was observed *in situ* in the presence of CO atmospheres, as indicated by the IR data in Figs. 3–5: detectable peaks are seen at 2137 and 2050 cm^{-1} at 295 and 495 K with $CuPt_{0.2}$/SBA-15, clearly originating from surface species and easily assignable to CO bonding to Cu and Pt sites, respectively. Additionally, the changes seen upon heating and cooling of the $CuPt_x$/SBA-15 catalysts are, again, reversible. It should be indicated that, in the catalysts containing high Pt loadings ($x \geq 0.05$), CO adsorption on Pt was seen at all temperatures; it is only with the diluted SAA catalysts ($x \leq 0.01$) that no surface Pt is detected at low temperatures and reversible segregation of Pt to the surface is clearly observed at high temperatures, possibly driven by bonding to CO. This does not indicate that segregation does not occur with the high-Pt-content catalysts, only that in those cases the behavior is masked by the combined response of the bimetallic NPs to changes in both temperature and CO pressure.

Complementary information could be extracted from *in situ* XAS experiments. The *in situ* XANES data reported in Fig. 7 for $CuPt_{0.2}$/SBA-15 does not show much change in the electronic structure of Pt as a function of temperature or the nature of the gas surrounding the surface of the catalyst. The main conclusion that can be driven there is that the features in the XANES traces with the bimetallic catalysts are much less defined than in pure Pt samples, suggesting good mixing with the Cu matrix and broadening of the Pt d band. On the other hand, analysis of the *in situ* EXAFS data in Figs. 8 and 9 does highlight a critical structural transition in $CuPt_{0.2}$/SBA-15 upon heating to 495 K. Specifically, the coordination sphere around the Pt atoms exhibit approximately the same number of Pt and Cu neighbors at low temperatures, but a significant increase in Cu–Pt bonds, at the expense of Pt–Pt pairs, is seen after heating to 495 K. This transition was observed under both reactive (CO) and un-reactive (He) atmosphere, and was found to be reversible, with the atoms redistributing back to their original configuration upon cooling back down to room temperature.

The high coordination number of Pt atoms bonding to other Pt atoms seen in $CuPt_{0.2}$/SBA-15 at low temperature indicates that Pt must form large ensembles within the bimetallic NPs. Two possible models can be conceived to explain the results: either Pt forms small clusters within the larger Cu–Pt NPs or it may form shells in a layered distribution of the metals within the NPs. The detection of CO adsorption in the IR experiments indicates that some Pt atoms are present on the surface of the catalyst at all temperatures, but the majority of the Pt may still be located in the sub-surface at low temperatures, perhaps separated by an intermediate Cu layer. After heating to 495 K, on the other hand, the CN for Pt–Pt pairs is significantly reduced, pointing to a better intermixing of the two metals. In addition, the CO IR peak associated with bonding to Pt becomes somewhat larger and sharper (Fig. 3), possibly because of a higher coverage of Pt on the surface but in a better dispersed fashion.

Old reports on the structure of Cu–Pt bimetallic samples can help with the interpretation of the data, in that: (1) Cu and Pt are completely miscible in both bulk and NP forms,[77] and (2) the superlattice of Cu–Pt alloys is characterized by successive alternating Cu-only and Pt-only layers.[78] More relevant to the understanding of our results, Cu–Pt alloys are known to transition from solid solutions at high temperatures to a number of ordered structures at low temperatures.[79,80] For an x = 0.2 composition (x being the Pt molar content in the $CuPt_x$/SBA-15 catalysts) this transition has been reported to take place at $T \geq 900$ K, but that is in bulk samples; the thermodynamics of NPs is expected to be different, and the interaction of the bimetallic NPs with gases may help lower the temperature of the transition even further. Interestingly, several layered structures with surface Pt rows and/or subsurface Pt sheets have been shown to be stable in $CuPt_x$ NPs by density-functional theory (DFT) calculations.[81,82] We therefore propose that our second explanation listed in the previous paragraph, where the Cu and Pt may segregate into alternating layers within the bimetallic NPs, may be the most likely. It should also be reiterated that the transitions reported here were seen with both CO and He atmospheres, which means that the strong binding of CO to Pt may not be the dominating force driving them.

Changes in surface chemistry due to the preferential segregation of one element in bimetallic NPs have been recognized in the past, as discussed in the Introduction, and some specific

examples have already been reported for Cu–Pt and similar cases. For instance, high-temperature CO-induced segregation of Pt atoms in Pt-doped Cu(111) surfaces has been identified by NAP-XPS.[38] The same behavior was seen with Pd/Ag(111),[43] but not with Pt/Cu(111) when H_2 is used instead of CO.[44] It is also interesting to note that no isotope scrambling within H_2 + D_2 mixtures was detected in experiments with $CuPd_x$ alloy films at any temperature below ~550 K until a ~15 mol. % Pd content was reached, a result that implies than no Pd atoms are accessible on the surface of diluted alloys for this catalysis.[23] Even under UHV, CO oxidation on Pt-doped O-dosed Cu(111) surfaces has been shown to lead to the diffusion of the Pt atoms to the layer underneath the Cu–O film,[83] a behavior consistent with our temperature-dependent IR observations reported in Figs. 1 and 2.

V. CONCLUSIONS

A synergy between Cu and Pt in Cu–Pt bimetallic catalysts was evidenced by their behavior both upon the uptake of CO under vacuum and during their exposure to atmospheric pressures of either CO or He. Under vacuum, CO adsorption on $CuPt_x$/SBA-15 catalysts only involves bonding to Cu sites at low (125 K) temperatures regardless of the Pt content (the x value), indicating the absence of Pt atoms on the surface (Fig. 1, left). Pt segregation becomes evident after heating to 225 K for $x \geq 0.2$ by the growth of a new peak in the IR spectra around 2044–2050 cm^{-1} (Fig. 1, second-from-left) but CO adsorption on those sites is still weaker than in pure Pt, desorbing at lower temperatures (Fig. 1, two right panels). The low IR frequency of the peaks for the Pt–CO sites suggest Pt atomic dispersion into small clusters (if not single atoms) on the surface, and the Pt segregation is partially reversible under the vacuum conditions of these experiments, as CO readsorption at room temperature leads to the disappearance of the IR feature for Pt–CO seen at the higher temperatures (Fig. 2).

Pt surface segregation at high (495 K) temperatures was also observed under a CO atmosphere, evidenced by the growth of a new peak around 2050 cm^{-1} in the *in situ* IR data (Fig. 3). The absence of CO adsorption at low temperatures and the reversibility of the Pt segregation to the surface at high temperatures are easy to see in diluted SAA $CuPt_x$/SBA-15 catalysts ($x \leq 0.01$; Fig. 4). With bimetallic catalysts having higher Pt content some Pt–CO sites can be detected even at low temperatures (Fig. 4), but some Pt diffusion in and out of the surface still occurs, only that it is highly dependent on temperature and the CO pressure used (Fig. 5). The possible Pt atom mobility within Cu–Pt NPs in the presence of H_2 atmospheres was also probed indirectly with *in situ* IR by adding small amounts of CO to the gas mixtures either during or after the thermal cycles (Fig. 6). The data are suggestive of Pt segregation aided by H_2, but this conclusion is not definitive because of a possible interference of the CO probe molecule during the *in situ* IR experiments.

Finally, the behavior of the $CuPt_{0.2}$/SBA-15 catalyst under CO and He atmospheres was also investigated by *in situ* by XAS. The near-edge region (XANES) of the spectra attested to the metallic and dispersed nature of the Pt atoms, and to an electronic structure not significantly affected by the presence of gases or temperature (Fig. 7). On the other hand, analysis of the extended structure (EXAFS; Fig. 8) highlighted a significant change in the coordination sphere around the Pt atoms upon heating of the catalyst. Specifically, the coordination numbers for neighboring Cu and Pt atoms switch from CN (Pt–Cu):(Pt–Pt) ratios of ~6:6 at 445 K or below to 8:4 at 495 K (Fig. 9), indicating better intermetallic mixing at high temperatures and possibly additional Pt segregation to the surface. Interestingly, the same behavior was seen with both CO and He, suggesting that the strong binding of CO to Pt may not be the main driving force justifying the diffusion reported here. It should be pointed out that information about the segregation of Pt atoms in between the bulk and the surface of bimetallic NPs is not easy to isolate with high-Pt-content catalysts because of the presence of some Pt atoms on the surface in those even at low temperatures. For that, work with more diluted SAAs is better. We are in the process of performing *in situ* IR and XAS experiments like those reported here with more diluted alloys.

SUPPLEMENTARY MATERIAL

See the supplementary material for metal loadings and average nanoparticle sizes of $CuPt_x$/SBA-15 catalysts and EXAFS fitting details.

ACKNOWLEDGMENTS

T.H. and F.Z. acknowledge financial support from the U.S. National Science Foundation, Division of Chemistry (Grant No. NSF-CHE1953843). A.I.F. acknowledges support from the U.S. National Science Foundation, Division of Chemistry (Grant No. NSF-CHE2203858). This research used the 8-ID (ISS) beamline of the National Synchrotron Light Source, a U.S. DOE Office of Science User Facilities operated for the DOE Office of Science by Brookhaven National Laboratory (BNL) under Contract No. DE-SC0012704. The authors thank the beamline scientist E. Stavitski at the 8-ID beamline of the NSLS-II for support during the beamline experiments.

AUTHOR DECLARATIONS

Conflict of Interest

The authors have no conflicts to disclose.

Author Contributions

Tongxin Han: Data curation (equal); Formal analysis (equal); Investigation (equal); Writing – review & editing (supporting). **Yuanyuan Li**: Data curation (equal); Formal analysis (equal); Investigation (equal); Writing – review & editing (supporting). **Yueqiang Cao**: Data curation (equal); Formal analysis (equal); Investigation (equal); Writing – review & editing (supporting). **Ilkeun Lee**: Data curation (supporting). **Xinggui Zhou**: Supervision (equal); Writing – review & editing (supporting). **Anatoly I. Frenkel**: Data curation (equal); Formal analysis (equal); Funding acquisition (equal); Investigation (equal); Supervision (equal); Writing – review & editing (supporting). **Francisco Zaera**: Conceptualization (lead); Data curation (lead); Formal analysis (lead); Funding acquisition (lead); Investigation (lead); Methodology (lead); Project administration (lead); Resources (lead); Supervision (lead); Writing – original draft (lead); Writing – review & editing (lead).

DATA AVAILABILITY

The data that support the findings of this study are available from the corresponding author upon reasonable request.

REFERENCES

[1] G. C. Bond, *Metal-Catalysed Reactions of Hydrocarbons*, Fundamental and Applied Catalysis (Springer, New York, 2005).
[2] D. Sanfilippo and P. N. Rylander, *Ullmann's Encyclopedia of Industrial Chemistry* (Wiley-VCH Verlag GmbH & Co. KGaA, Weinheim, 2012), p. 451.
[3] Z. Ma and F. Zaera, in *Encyclopedia of Inorganic and Bioinorganic Chemistry*, edited by R. A. Scott (John Wiley & Sons, Chichester, 2014), p. eibc0079.
[4] J. H. Sinfelt, *Bimetallic Catalysts: Discoveries, Concepts and Applications* (John Wiley & Sons, New York, 1983).
[5] R. Ferrando, J. Jellinek, and R. L. Johnston, Chem. Rev. **108**, 845 (2008).
[6] W. Yu, M. D. Porosoff, and J. G. Chen, Chem. Rev. **112**, 5780 (2012).
[7] J. A. Rodriguez, Surf. Sci. Rep. **24**, 223 (1996).
[8] Y. Wang and P. B. Balbuena, J. Phys. Chem. B **109**, 18902 (2005).
[9] A. J. Medford *et al.*, J. Catal. **328**, 36 (2015).
[10] M. T. Greiner *et al.*, Nat. Chem. **10**, 1008 (2018).
[11] V. Ponec, Appl. Catal. A **222**, 31 (2001).
[12] P. Liu and J. K. Nørskov, Phys. Chem. Chem. Phys. **3**, 3814 (2001).
[13] F. Gao and D. W. Goodman, Chem. Soc. Rev. **41**, 8009 (2012).
[14] S. Sarfraz *et al.*, ACS Catal. **6**, 2842 (2016).
[15] P. N. Duchesne *et al.*, Nat. Mater. **17**, 1033 (2018).
[16] J. Han *et al.*, Chin. J. Chem. **37**, 977 (2019).
[17] R. T. Hannagan *et al.*, Chem. Rev. **120**, 12044 (2020).
[18] F. Zaera, Chem. Rev. **122**, 8594 (2022).
[19] M. Johansson, O. Lytken, and I. Chorkendorff, J. Chem. Phys. **128**, 034706 (2008).
[20] L. Álvarez-Falcón *et al.*, Surf. Sci. **646**, 221 (2016).
[21] B. Chen and F. Zaera, J. Phys. Chem. C **125**, 14709 (2021).
[22] C. P. O'Brien *et al.*, J. Phys. Chem. C **115**, 24221 (2011).
[23] G. Gumuslu *et al.*, ACS Catal. **5**, 3137 (2015).
[24] M. Luneau *et al.*, Chem. Rev. **120**, 12834 (2020).
[25] E. C. H. Sykes and P. Christopher, Curr. Opin. Chem. Eng. **29**, 67 (2020).
[26] M. B. Boucher *et al.*, Phys. Chem. Chem. Phys. **15**, 12187 (2013).
[27] F. R. Lucci *et al.*, Nat. Commun. **6**, 8550 (2015).
[28] G. X. Pei *et al.*, ACS Catal. **7**, 1491 (2017).
[29] M. Luneau *et al.*, ACS Catal. **10**, 441 (2019).
[30] Y. Cao *et al.*, ACS Catal. **9**, 9150 (2019).
[31] Y. Cao *et al.*, ACS Catal. **10**, 3431 (2020).
[32] F. R. Lucci *et al.*, J. Phys. Chem. C **119**, 24351 (2015).
[33] M. T. Darby *et al.*, J. Phys. Chem. Lett. **9**, 5636 (2018).
[34] G. Giannakakis, M. Flytzani-Stephanopoulos, and E. C. H. Sykes, Acc. Chem. Res. **52**, 237 (2019).
[35] M. T. Darby *et al.*, ACS Catal. **8**, 5038 (2018).
[36] H. Thirumalai and J. R. Kitchin, Top. Catal. **61**, 462 (2018).
[37] J. Schumann *et al.*, J. Phys. Chem. Lett. **12**, 10060 (2021).
[38] J. P. Simonovis *et al.*, J. Phys. Chem. C **122**, 4488 (2018).
[39] D. Molina and M. Trenary, in *AVS 68th International Symposium and Exhibition* (American Vacuum Society, Pittsburgh, PA, 2022).
[40] S. Zafeiratos, S. Piccinin, and D. Teschner, Catal. Sci. Technol. **2**, 1787 (2012).
[41] K. G. Papanikolaou, M. T. Darby, and M. Stamatakis, J. Phys. Chem. C **123**, 9128 (2019).
[42] S. Liu *et al.*, ACS Catal. **9**, 5011 (2019).
[43] M. A. van Spronsen *et al.*, J. Phys. Chem. C **123**, 8312 (2019).
[44] J. P. Simonovis *et al.*, Surf. Sci. **679**, 207 (2019).
[45] F. Tao *et al.*, Science **322**, 932 (2008).
[46] Z. Konuspayeva *et al.*, J. Mater. Chem. A **5**, 17360 (2017).
[47] E. V. Carino and R. M. Crooks, Langmuir **27**, 4227 (2011).
[48] N. Marcella *et al.*, Nat. Commun. **13**, 832 (2022).
[49] H. Tiznado, S. Fuentes, and F. Zaera, Langmuir **20**, 10490 (2004).
[50] F. Zaera, ChemCatChem **4**, 1525 (2012).
[51] P. J. Chupas *et al.*, J. Appl. Crystallogr. **41**, 822 (2008).
[52] M. Kohler *et al.*, J. Catal. **117**, 188 (1989).
[53] A. Dandekar and M. A. Vannice, J. Catal. **178**, 621 (1998).
[54] K. Hadjiivanov and H. Knözinger, Phys. Chem. Chem. Phys. **3**, 1132 (2001).
[55] D. J. Stacchiola, Acc. Chem. Res. **48**, 2151 (2015).
[56] N. D. Nielsen *et al.*, Surf. Sci. **703**, 121725 (2021).
[57] T. Han *et al.*, J. Phys. Chem. C **126**, 3078 (2022).
[58] R. A. Shigeishi and D. A. King, Surf. Sci. **58**, 379 (1976).
[59] R. Martin, P. Gardner, and A. M. Bradshaw, Surf. Sci. **342**, 69 (1995).
[60] F. Zaera, J. Liu, and M. Xu, J. Chem. Phys. **106**, 4204 (1997).
[61] M. J. Kappers and J. H. van der Maas, Catal. Lett. **10**, 365 (1991).
[62] J. Liu *et al.*, J. Am. Chem. Soc. **138**, 6396 (2016).
[63] J. Finzel and P. Christopher, Top. Catal. **65**, 1587 (2022).
[64] M. T. Darby *et al.*, Top. Catal. **61**, 428 (2018).
[65] C. T. Campbell *et al.*, Surf. Sci. **107**, 207 (1981).
[66] J. L. Gland and E. B. Kollin, J. Chem. Phys. **78**, 963 (1983).
[67] B. Tränkenschuh *et al.*, Surf. Sci. **601**, 1108 (2007).
[68] G. Sun *et al.*, Nat. Commun. **9**, 4454 (2018).
[69] B. E. Hayden and A. M. Bradshaw, Surf. Sci. **125**, 787 (1983).
[70] B. E. Hayden *et al.*, Surf. Sci. **149**, 394 (1985).
[71] J. A. Rodriguez, C. M. Truong, and D. W. Goodman, J. Chem. Phys. **96**, 7814 (1992).
[72] A. M. Baró, H. Ibach, and H. D. Bruchmann, Surf. Sci. **88**, 384 (1979).
[73] Ş. C. Bădescu *et al.*, Phys. Rev. Lett. **88**, 136101 (2002).
[74] H. Asada *et al.*, J. Chem. Phys. **63**, 4078 (1975).
[75] A. J. Renouprez and H. Jobic, J. Catal. **113**, 509 (1988).
[76] S. F. Parker *et al.*, Chem. Eur. J. **25**, 6496 (2019).
[77] G. Meitzner *et al.*, J. Chem. Phys. **83**, 353 (1985).
[78] R. S. Irani and R. W. Cahn, Nature **226**, 1045 (1970).
[79] T. Abe, B. Sundman, and H. Onodera, J. Phase Equilib. Diffus. **27**, 5 (2006).
[80] Y. Liu, L. Zhang, and D. Yu, J. Phase Equilib. Diffus. **30**, 136 (2009).
[81] J. Tang *et al.*, J. Phys. Chem. C **119**, 21515 (2015).
[82] L. Vega *et al.*, Mater. Adv. **2**, 6589 (2021).
[83] A. J. Therrien *et al.*, Nat. Catal. **1**, 192 (2018).